1   **Supplementary Materials**

2   **Experimental setup**
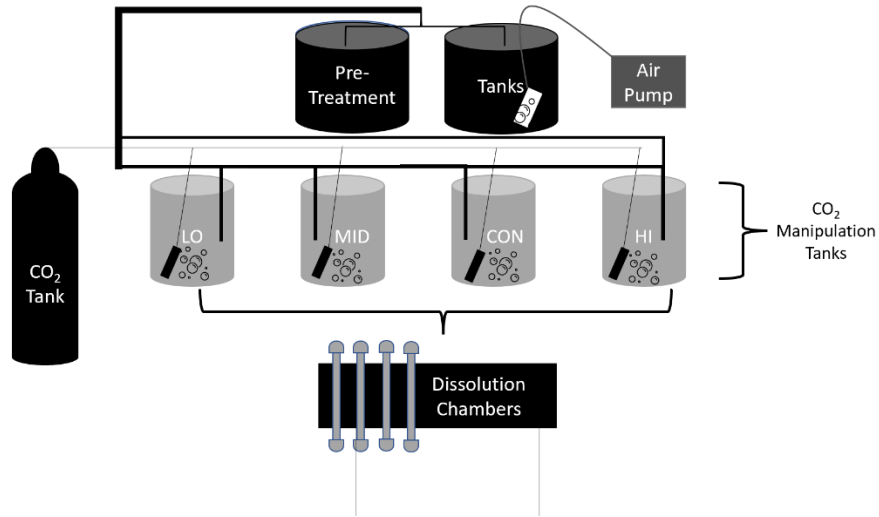
6   **Figure S1:** Simplified schematic of the flow through feedback-controlled seawater system used
7   for the mineral dissolution experiments. The pre-treatment tanks contained seawater filtered to 5
8   microns from Yaquina Bay and were vigorously bubbled with ambient air. Water was pumped
9   from the pre-treatment tanks to the CO_2 manipulation tanks (Lo, Mid, Con, Hi) and excess water
10   was then circulated back. CO_2 treatment tanks were manipulated using lab-grade CO_2 to generate
11   specific $\Omega_{calcite}$ in a feedback-controlled system measuring $pH_{(NBS)}$. The pH in each CO_2
12   manipulation tank was monitored using an Apex-Controller manipulation system (Neptune
13   Systems Energy Bar 832 interfaced with an Apex Controller Base Unit and pH/ORP probe
14   modules: PM1). One double junction pH probe was located in the recirculation return line in each
15   CO_2 manipulation tank. All pH probes were calibrated at the beginning of each experiment using
16   pH 4, 7, and 10 NBS buffers, to obtain a three-point calibration curve.

17

18   **Table S1:** Table of measured TCO_2, pCO_2, Temperature (T), Salinity (S) and calculated pH_{NBS}
19   and Saturation State ($\Omega_{calcite}$) from seawater tank discrete (pCO_2/TCO_2) samples associated with
20   our flow through feedback-controlled seawater system. For each dissolution trial, a total of four
21   pCO_2/TCO_2 samples were used. Measurements following procedures from Bandstra et al. (2006),
22   modified for discrete samples as in Hales et al. (2005), Barton et al., (2012), and Hales et al. (2017).
23   The temperature (^{o}C) listed is from in situ measurements recorded from within the water treatment
24   tanks (does not reflect experimental temperatures)

TCO_2 (µmol/kg)	pCO_2 (µatm)	T (^{o}C)	Salinity	Measured pH_{NBS}	Calculated $\Omega_{calcite}$

2530.7	8589.3	18	33.1	6.85	0.25
2340.1	4569.2	18	33.2	7.14	0.45
2291.5	2537.9	19	33.4	7.28	0.85
2252.8	1946.2	18	33.2	7.46	1.03

25

26 The correlation between measured benchtop pH data and the pH data calculated from pCO_2/TCO_2
27 measurements for header tanks in all experiments was consistently an R^2 greater than 0.9 across
28 all experiments (Figure S2).
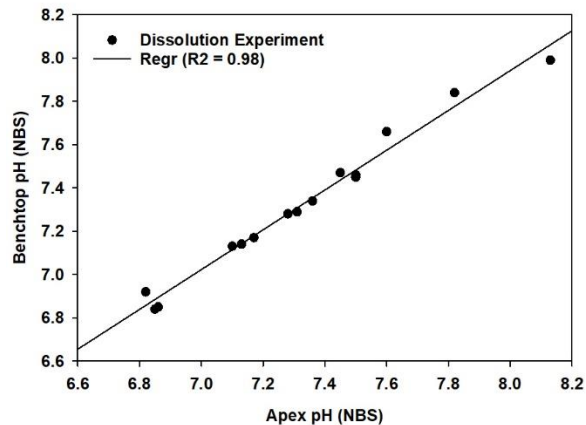
29

30 **Figure S2**: Measured pH_{NBS} from a benchtop probe and the pH_{NBS} from the experimental system
31 in the flowthrough feed-back controlled seawater system tanks

32

33 *Effect of the dilution due to mineral addition*

34 We carried out addition simulations in which we assumed that the addition of minerals at the top
35 replaces OM, lowering the OM concentration in the top 2 cm. To estimate the potential impact
36 of dilution due to replacing OM with PIC, we simulated OM as state variable and using a rate
37 expression $R_C = k*OM$, replacing the imposed OM reaction rates $R_C = R_C^0 *exp(-x/g_{om})$. We
38 assumed that the proportion of addition of PIC is the same as removal of the OM (i.e., adding 8%
39 of mineral means lowering OM concentration by 8%). The rate constant k was set to 0.25 yr^{-1},
40 chosen to approximate the rates computed in the $R_C(z)$ approach. Flux of carbon was taken from
41 literature as ~510 μmol cm^{-2} yr^{-1} (Thullner et al., 2009).

42 Figure S3 shows before and after the addition of minerals when dilution is present. We compared
43 these results against a simulation with dilution turned off. Impact of dilution was minimal with
44 slight reductions observed mainly in OM mineralization processes which resulted in decreases in
45 TA production rates. Production of TA production was reduced by 17 and 33 μmol cm^{-2} yr^{-1} for
46 8% and 16% applications respectively.
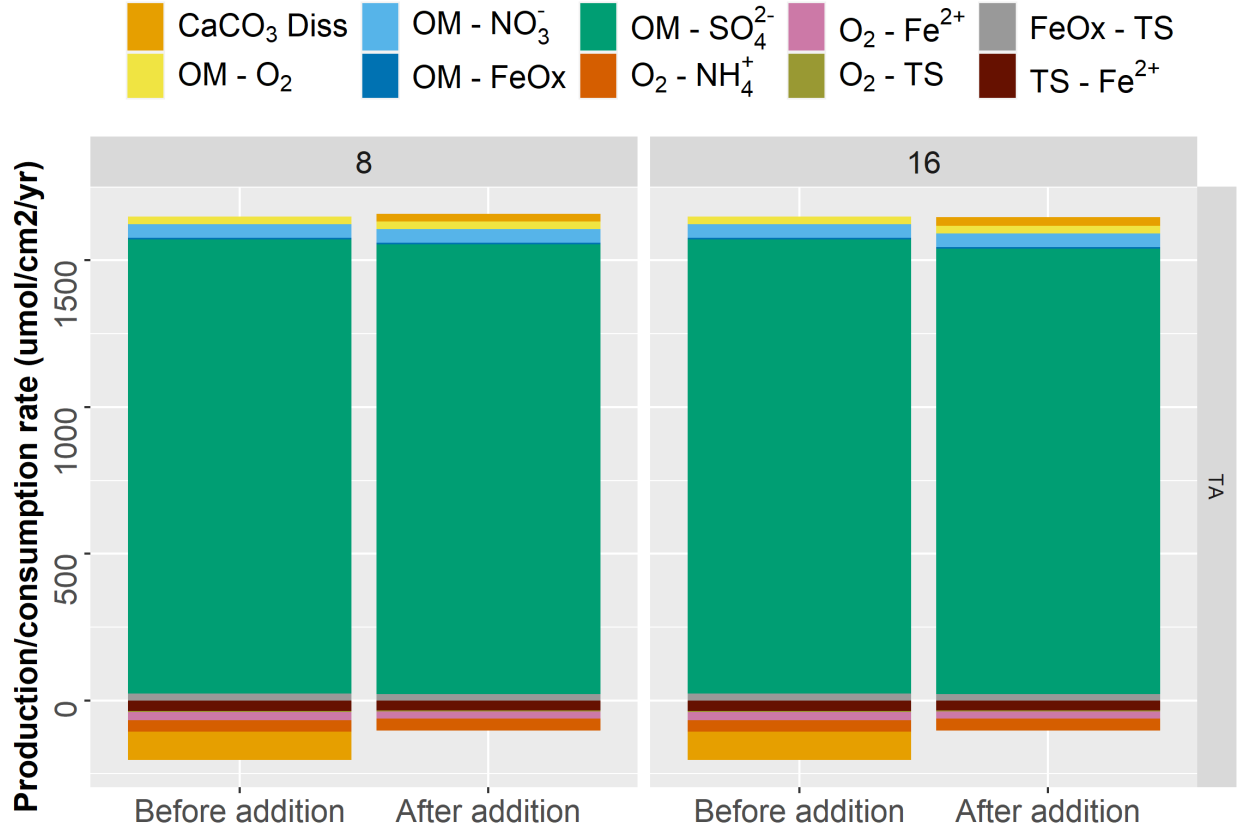
Figure S3. Production of TA for different amounts of mineral added when dilution is considered (8 = 8% mineral addition, 16 = 16% mineral addition).

Box model for atmospheric DIC uptake

To estimate the impact of OAE on benthic fluxes calculated in this study and thus CO_2 uptake in Yaquina Bay, we used a simple mass balance approach similar to Brenner et al. (2016), which focuses on the ratio of DIC over TA as the controlling factor of CO_2 uptake (Egleston et al., 2010). We calculated the mass balance for TA and DIC prior to and 2 years after the mineral addition to isolate the additional CO_2 uptake due to mineral addition. Riverine impact was assumed negligible, reflecting the strong coupling of Yaquina Bay with the coastal ocean reported previously (Brown & Ozretich, 2007). Therefore, tidal exchange and benthic fluxes were the only input/output pathways considered in the TA mass balance (Figure S4). At steady state, the alkalinity balance is given by:

$$F_i^{TA} - F_o^{TA} + F_b^{TA} + R^{TA} = 0$$

where F_i^{TA} is the tidal influx of TA as a function of water exchange rate and oceanic TA ($F_i^{TA} = v[TA_{ocean}]$), F_o^{TA} is the tidal outflux of TA from the Bay to the ocean as a function of tidal velocity and TA of the study site ($F_o^{TA} = v[TA_{site}]$), F_b^{TA} is the benthic flux computed by the reactive transport model and R^{TA} is the net rate of water column TA production/consumption resulting from primary productivity and respiration. The mass balance for DIC is given by:

$$F_i^{DIC} - F_o^{DIC} + F_b^{DIC} + F_a^{DIC} + R^{DIC} = 0$$

67 where F_i^{DIC} is the tide-driven influx of DIC ($F_i^{DIC} = v[DIC_{ocean}]$), F_o^{DIC} is the outflux of DIC

68 ($F_o^{DIC} = v[DIC_{site}]$), F_b^{DIC} is the benthic flux of DIC, F_a^{DIC} is the atmospheric CO_2 and R^{DIC} is the

69 sum of reaction rates producing/consuming DIC.
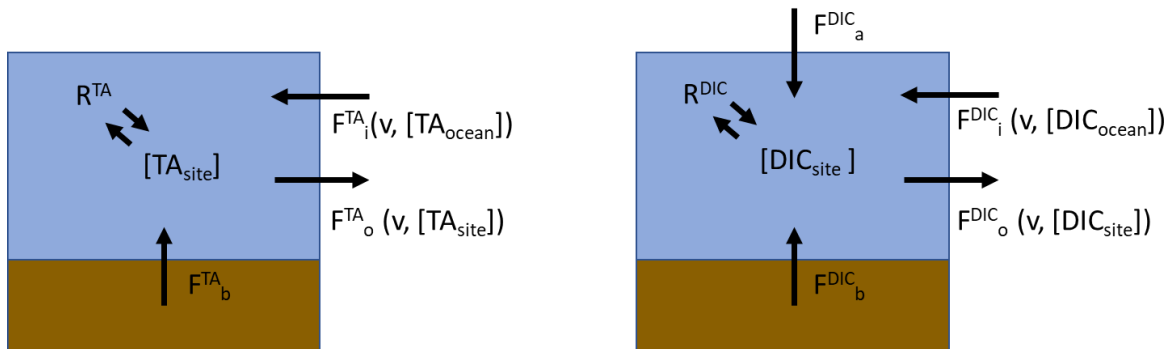
70

71 **Figure S4:** Schematic of water column TA and DIC fluxes for Yaquina Bay.

72 The water exchange rate was approximated from measurements of water height. Using a 3 m

73 semidiurnal tidal range from NOAA South Beach, OR (Station ID: 9435380) station, a

74 representative exchange velocity is $2.1 \ast 10^5$ cm/yr .

75 For pre-addition scenario, benthic TA and DIC fluxes were taken from the model as 1100 and

76 1121 µmol cm^{-2} yr^{-1} respectively. TA mass balance equation was solved for R^{TA} using $[TA_{ocean}]$

77 as 2.2 and $[TA_{site}]$ as 1.9 mmol L^{-1} (measured at Hatfield Marine Station). Then, R^{DIC} was

78 estimated using R^{TA} with respiration producing NO_3^-/primary production consuming NO_3^-

79 (coupled respiration and nitrification). $[DIC_{site}]$ and $[DIC_{ocean}]$ were calculated using site and

80 ocean TA and pH using aquaenv R package as 1.8 and 2.1 µmol/cm^{-3} respectively. Lastly, F_a^{DIC}

81 was estimated by DIC mass balance.

82 After the addition of minerals, benthic fluxes were 1227 and 1185 µmol cm^{-2} yr^{-1} for TA and DIC.

83 $[TA_{site}]$ and $[DIC_{site}]$ were recalculated using mass balance with R^{TA}, R^{DIC} , assuming pH of the

84 site to be constant from pre-addition and changes in $[TA_{site}]$ and $[DIC_{site}]$ were in the order of

85 10^{-3} µmol/cm^3.

86 Flux of CO_2 between the atmosphere and the water showed that the bay is net heterotrophic with

87 emission fluxes of 458352 and 458294 µmol cm^{-2} yr^{-1} for before and after the addition respectively.

88 Impact of buffering on F_a^{DIC} was calculated as additional 58 µmol cm^{-2} yr^{-1} CO_2 flux into the water

89 column during the peak buffering period which was significantly smaller than total CO_2 influxes

90 due to large impact of tidal input.

91 We explored the sensitivity of air-sea CO_2 fluxes to the pH in the bay, as well as the magnitude of

92 the tidal exchange between the bay and the coastal ocean. CO_2 uptake due to mineral addition was

93 slightly sensitive to pH in the bay (a change of approximately 14 µmol cm^{-2} yr^{-1} per change in 1

94 pH unit). However, since the CO_2 uptake due to mineral additions were calculated as the difference

95 between two scenarios, altering the tidal input (tidal exchange volume, DTA, DDIC) did not have

96 a considerable impact on the impact of buffering (not shown).

References:

Bandstra, L., Hales, B., & Takahashi, T. (2006). High-frequency measurements of total CO2: Method development and first oceanographic observations. Marine Chemistry, 100(1-2), 24-38.

Barton, A., Hales, B., Waldbusser, G. G., Langdon, C., & Feely, R. A. (2012). The Pacific oyster, Crassostrea gigas, shows negative correlation to naturally elevated carbon dioxide levels: Implications for near-term ocean acidification effects. Limnology and oceanography, 57(3), 698-710.

Brown, C. A., & Ozretich, R. J. (2009). Coupling between the coastal ocean and Yaquina Bay, Oregon: Importance of oceanic inputs relative to other nitrogen sources. Estuaries and Coasts, 32, 219-237.

Hales, B., Suhrbier, A., Waldbusser, G. G., Feely, R. A., & Newton, J. A. (2017). The carbonate chemistry of the "fattening line," Willapa Bay, 2011–2014. Estuaries and Coasts, 40, 173-186.

Hales, B., Takahashi, T., & Bandstra, L. (2005). Atmospheric CO2 uptake by a coastal upwelling system. Global Biogeochemical Cycles, 19(1).

Thullner, M., Dale, A. W., & Regnier, P. (2009). Global-scale quantification of mineralization pathways in marine sediments: A reaction-transport modeling approach. Geochemistry, geophysics, geosystems, 10(10).